AIAA AVIATION Forum
August 2-6, 2021, VIRTUAL EVENT
AIAA AVIATION 2021 FORUM

10.2514/6.2021-2859

Static Wall Pressure Measurements of Supersonic Underexpanded Jet Impingement

Hussein Al-Rashdan*, Nicolas Rasmont†, Joshua Rovey‡, Gregory Elliott§, Laura Villafane-Roca¶
University of Illinois at Urbana-Champaign, Urbana, IL, 61801

This paper summarizes an experimental study of an underexpanded, axisymmetric jet impinging on a solid flat plate at Lunar and Martian atmospheric conditions for a varying nozzle-to-impingement surface distance. The jet angle of incidence is maintained at 90°, the ideal landing condition for a payload with a central retrograde rocket. Tests have shown that large transient pressure spikes with amplitudes ranging from between 6.1 and 8.8 kPa for Lunar impingement and between 17.2 and 39.7 kPa for Martian impingement form on the surface of the flat plate. Pressure spike duration is directly proportional to the startup and shutdown rates of the pulsed supersonic jet and corresponds to the formation or collapse of a strong normal plate shock above the surface. Schlieren imaging corroborates this result by correlating flow structure dynamics at the plate with surface pressure measurements. Experimental measurements show that peak steady state surface pressure has a nonlinear response to the impingement distance for jets that are moderately underexpanded (the nozzle exit pressure to ambient pressure ratio is on the order of 2-3). Large transient pressure spikes can create explosive erosion events that can rapidly deplete the soil beneath a lander, introducing the risk of unstable landing and the scouring of nearby objects. Our goal is to better understand the complex coupled multiphysics that occurs within the interactions of a supersonic jet, the cratering surface, and the eroding topsoil. Characterizing the flow dynamics and impingement pressure distribution at incremental points during the terminal descent stage of EDL forms the starting basis for this goal.

I. Nomenclature

R_t	=	throat radius
R_e	=	exit radius
D_t	=	throat diameter
D_e	=	exit diameter
h	=	impingement height
JPR	=	Jet pressure ratio
γ	=	specific gas ratio
M_1	=	Mach number upstream from a normal plate shock
P_{01}	=	Total pressure upstream of a normal plate shock
P_{02}	=	Total pressure downstream of a normal plate shock
P_{amb}	=	Vacuum ambient pressure

II. Introduction

In In recent years, NASA has been charged with returning astronauts to the Moon and expanding its robotic presence on Mars. These types of large-scale interplanetary missions require spacecraft with powerful descent engines to necessarily impinge on the surface of regolith laden bodies. This terminal descent stage of Entry, Descent, and Landing

*PhD Candidate, Aerospace Engineering, 324 Talbot Laboratory, 104 South Wright St., AIAA Student Member.
†PhD Candidate, Aerospace Engineering, 324 Talbot Laboratory, 104 South Wright St., AIAA Student Member.
‡Associate Professor, Aerospace Engineering, 317 Talbot Laboratory, 104 South Wright St., AIAA Associate Fellow.
§Professor, Aerospace Engineering, 301 Talbot Laboratory, 104 South Wright St., AIAA Associate Fellow.
¶Assistant Professor, Aerospace Engineering, 313 Talbot Laboratory, 104 South Wright St., AIAA Member.

(EDL) introduces a unique set of challenges and hazards to the overall success of a mission. The potential hazards can include: the lifting of particulates obstructing the vision of the landing craft and its occupants, high velocity granular erosion damaging nearby assets and the landing craft itself, and surface cratering destabilizing the landing topology. It is necessary to better understand the impingement process and the physical dynamics that govern it as this will allow us to develop predictive capabilities that can drive engineering controls and design decisions.

One of the focuses in plume surface interaction (PSI) studies involve the investigation of the coupled multi-physics phenomena arising in the interactions between a descent lander jet and the soil laden surface of a gravitational body existing under a given set of ambient and soil conditions. In order to conduct a series of well controlled plume-surface impingement experiments that replicate the main non-dimensional aerodynamic parameters of relevant gravitational bodies, subatmospheric conditions must be generated. The reasons are twofold: the exhaust plume of a subscale thruster must be sufficiently underexpanded to match the aerodynamic scaling parameters, and the aerodynamic body forces experienced by ejected particles must be commensurate with real world particle ejection [1].

Investigating the surface loads on a particle laden surface is difficult due to the transient nature of the interactions between the particulate surface, the jet, and the surrounding quiescent gas. As the jet erodes the surface of the soil floor, the forming crater introduces a new impingement geometry which in turn modifies the flow of the jet. Additionally, high particle loading caused by erosion at the crater walls and soil lifting in the stagnation recirculation bubble complicate the process of measuring the contribution of the crater geometry to the modification of the jet flow. A method of decoupling the crater geometry from the soil medium will be explored with a starting point of impinging a jet onto an uncratered flat plate.

III. Experimental Apparatus

A GNB Corporation vacuum chamber, 2375 liters in volume, was used to house the supersonic nozzle, impingement plate, and the schlieren optical components that form the experimental testbed of this study. The chamber was fitted with a custom made door with a large optical access window. This window provided an exceptional field of view into the vacuum chamber and flexibility in the imaging of the test section. A thruster subassembly comprised of a converging-diverging nozzle, solenoid valve, plenum thermocouple, and plenum pressure transducer was fitted into the vacuum chamber and linked to an external gas supply via a gas feedthrough. Once the conditions for underexpanded flow have been met, the thruster is activated and the jet impinges on the target surface.

The following subsections outline in detail the design and operational parameters for the cold gas thruster as well as the design of the two measurement techniques, namely the impingement plate embedded with pressure sensors and the schlieren imaging setup. This section will conclude with a discussion on the data acquisition and synchronization system.

A. Cold Gas Thruster

Dry compressed nitrogen gas was chosen to simulate the hydrazine decomposition products of a retrograde rocket due to their similar specific heat capacity [2]. Commercial nitrogen bottles feed a 20-gallon reservoir tank with a high coefficient of flow connection to the nozzle (Figure 1), ensuring the mass flow rate becomes choked at the throat location in the converging-diverging nozzle and not upstream in the feedline. Pressure and temperature in the plenum are monitored by a K-type thermocouple and an Omega PX309 absolute pressure transducer located directly upstream of the nozzle entrance, as seen in Figure 2a. These locations ensure that the stagnation properties of the gas are accurately gauged before the gas is accelerated through the nozzle. The ambient vacuum pressure is monitored by an MKS capacitive manometer and a Lesker cold-cathode Pirani gauge.

A converging-diverging axisymmetric nozzle was used to generate the impingement jet. The geometry consists of a circular converging section with an inlet radius of 1.5 throat radii, R_t, similar to bell nozzles designed using the Method of Rao contour [3]. The nozzle converges to a throat radius of 1 mm before transitioning into a parabolic expansion section designed using the method of characteristics to generate waveless flow within the expansion section. The exit radius, R_e, is 5 mm and results in an expansion area ratio of 25 which in turn produces an exit Mach number of 5.0. The nozzle was manufactured by Stratasys-Direct using a Direct Metal Laser Sintering (DMLS) fabrication technique out of stainless steel 304.

The pressure in the nozzle plenum is set to 1.2 MPa to match the jet pressure ratio, JPR, exhibited by a Martian lander [4]. By varying the ambient pressure in the vacuum chamber between 6 Torr and 50 mTorr, the nozzle operates at jet pressure ratios of 2.84 and 340, which represent the approximate exit-to-ambient pressure expansion ratio at the Martian and Lunar surfaces, respectively. Both the reservoir and plenum in this set of experiments were unheated and

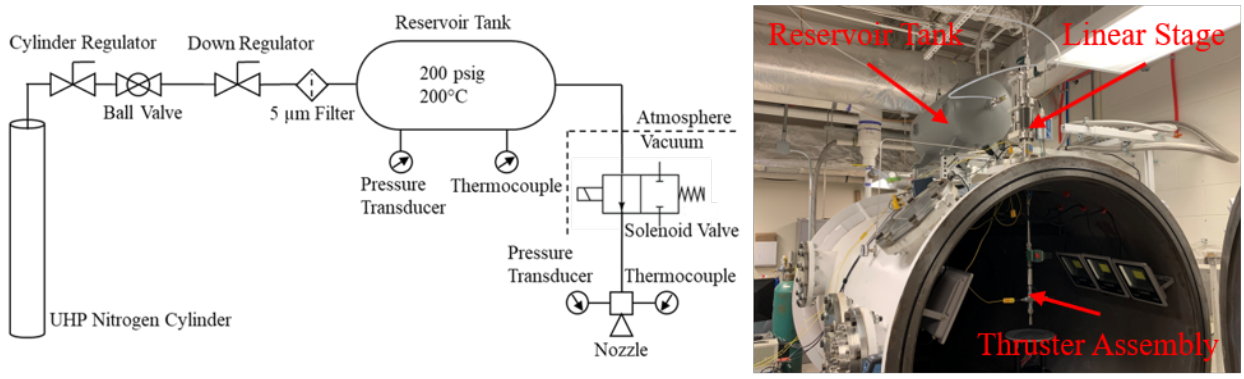

Fig. 1 Mach 5 nozzle and feedline schematic for flat plate impingement(left) and laboratory view of cold gas thruster implementation(right).

operating at lab temperature, 300K. As a result, the exit temperature is predicted to be 50K. There was concern that this low exit temperature could lead to the freezing of the nitrogen propellant which has a freezing point of 63 K at a pressure of one atmosphere. This did not occur due to the low vacuum ambient pressure and nitrogen solids were not observed forming in the imaging process. By measuring the stagnation temperature, stagnation pressure, and ambient pressure the remaining flow conditions can be estimated using compressible flow theory governing supersonic nozzle flow. These are summarized in Tables 1 and 2 alongside the parameters for the Phoenix rocket motor.

Table 1 Dimensional flow conditions of Mach 5 nozzle as compared to full scale retrograde rockets.

Parameter	Lab Scale	Full Scale
Exit Pressure (Pa)	2268.04	3240
Ambient Pressure (Pa)	6.7-800	0-858
Exit Velocity (m/s)	720.69	1929
Exit Temperature (K)	50	3300
Exit Viscosity (Pa-s)	$3.15 * 10^{-6}$	$9.4 * 10^{-6}$
Mean Free Path (μm)	0.517	6000
Mass Flow Rate (g/s)	8.65	320

Table 2 Non-Dimensional flow conditions of Mach 5 nozzle as compared to full scale retrograde rockets.

Parameter	Lab Scale	Full Scale
Mach Number	5.0	4.7
Jet Pressure Ratio	2.84-340	3.8
Reynolds Number	$3.49 * 10^{5}$	$3.4 * 10^{5}$
Knudsen Number	$51.68 * 10^{-6}$	0.03

The flow is controlled by a normally closed solenoid valve located directly upstream of the nozzle plenum. Energizing the coil in the solenoid opens the valve and connects the large reservoir tank located in the lab to the thruster assembly located within the vacuum chamber. Once energized, the plenum is supplied with gas and pressurized at a rate of 175.91 MPa/s until the design stagnation pressure of 1.2 MPa is achieved, approximately 18 milliseconds after the opening signal is issued. The nozzle is pulsed open for one-second, which is motivated by the requirement of minimizing the amount of ambient pressure drift. After the signal to close the valve is issued, the combined time for the solenoid to fully close and for the gas in the plenum to empty is approximately 88 milliseconds. This results in an approximately square stagnation pressure curve, which is easy to simulate should the results be explored further in computational models.

The thruster subassembly is mounted on a single-axis linear stage capable of 15.0 cm of travel. The linear stage is manually operated so that the nozzle position, relative to the impingement surface, is read from a graduated scale etched into the instrument. This results in a ±0.5 mm uncertainty in the height of the nozzle exit above the plate. In the future, motorizing this stage and utilizing a rotary encoder can reduce this uncertainty.

B. Flat 90° Impingement Plate

A low tolerance MIC-6 aluminum plate eight inches in diameter was chosen as the impingement target due to the cast alloy having a better degree of flatness and surface consistency over more common metals. Five NXP micro-electromechanical, MEM, piezoresistive pressure sensors are placed in a row along the centerline chord of the impingement plate, equidistant at a pitch of 8 mm, (Figure 2). The target plate is rigidly attached to an adjustable height stage which aids in the zeroing of the cold gas thruster linear stage between test runs as described in Section IV.

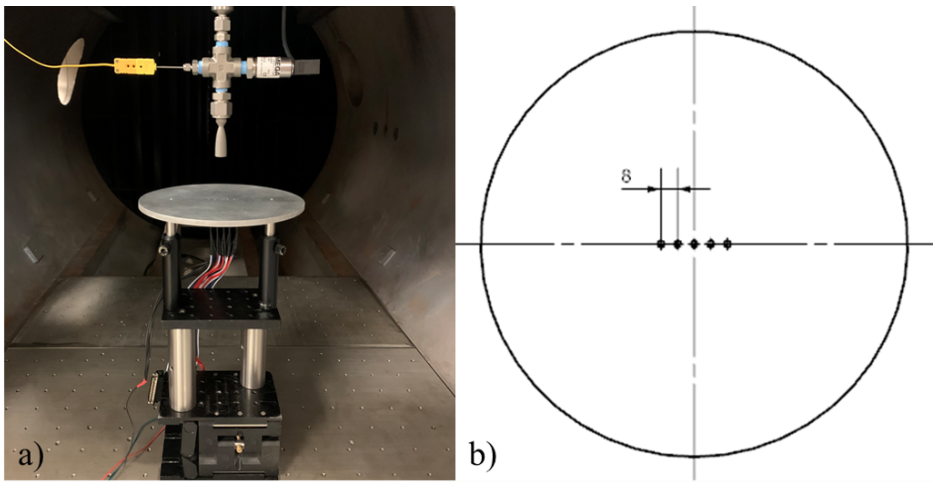

Fig. 2 a) Impingement plate supported on an adjustable height stage beneath the cold gas thruster. b) Top view schematic of sensor arrangement and spacing.

The operating range of the MEM sensors was determined using 1D normal shock relations that govern the behavior of the flow along the centerline of the axisymmetric jet. When the JPR is greater than unity, the gas exit pressure is greater than the surrounding ambient pressure. In such a case, the flow out of the nozzle is expanded outwards through an expansion fan, developing a radial component of velocity and reducing in pressure. Streamlines with a radial velocity component will expand to meet the free pressure boundary that develops when the jet and the surrounding quiescent gas form a pressure matched slip line [5]. In contrast, due to the radial symmetry of the jet, purely axial flow along the nozzle centerline will continue to propagate in one direction.

When the impingement height is low, $h = D_e$, the flow undergoes very little expansion and axial acceleration. This scenario can be modeled as a 1D, Mach 5 flow being processed by a strong normal plate shock before being isentropically decelerated to stagnation at the pressure sensor. The centerline impingement pressure in this test case is then governed by the total pressure loss across the normal shock wave and formally serves as an upper bound from which the MEMS piezoresistive sensors were selected. The total pressure loss across a normal shock is:

$$\frac{P_{02}}{P_{01}} = \left(\frac{\frac{\gamma+1}{2} M_1^2}{1 + \frac{\gamma-1}{2} M_1^2} \right)^{\frac{\gamma}{\gamma-1}} \left(\frac{2\gamma}{\gamma+1} M_1^2 - \frac{\gamma-1}{\gamma+1} \right)^{\frac{-1}{\gamma-1}} \tag{1}$$

where γ is the specific gas ratio of the component gas, M_1 is the upstream Mach number prior to normal shock processing, and P_{0x} is the total pressure of the upstream and downstream flow (subscript 1 and 2, respectively). With a theoretical upstream Mach number of 5.0 and the specific gas ratio of nitrogen $\gamma = 1.4$, the total pressure ratio across the plate shock can be found, $P_{02}/P_{01} = 0.0617$. The plenum total pressure noted in Section A results in an estimated centerline wall pressure of 74.06 kPa at a low impingement height. This wall pressure data point helped to select MEMS piezoresistive pressure sensors with a measurement range of 0-100 kPa. NXP MEMS sensors were chosen due to their low cost and small form factor, as well as being temperature compensated and accurate to within 2.6% of their factory

calibration. In practice, a jet impingement at $h = D_e$ agrees with the analytical estimate given in Equation 1 and is accurate to within 0.07% to 2.5% depending on the initial ambient conditions as shown in Figure 3. One drawback of these commercial sensors is that with a response time of one millisecond, impingement transients with a frequency component greater than ~500 Hz cannot be adequately sampled and reconstructed.

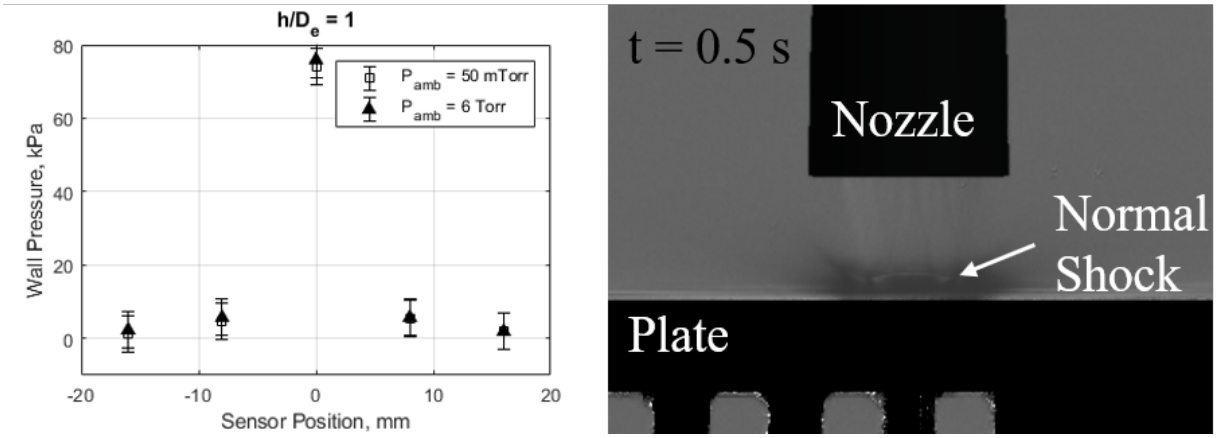

Fig. 3 a) Equilibrium wall static pressure distribution for $h = D_e$ at both P_{amb} = 50 mTorr (Lunar atmosphere) and P_{amb} = 6 Torr (Martian atmosphere). b) Instantaneous image from schlieren recording at t = 0.5 seconds demonstrating the plate shock, P_{amb} = 50 mTorr.

C. Schlieren Imaging

Imaging of the impinging flow structure was performed using a Herschellian schlieren system [6] with the nozzle axis located at the center of a 2 meter long path of collimated light. Two 6 inch f/10 spherical mirrors were arranged in the standard Z-configuration, as laid out in Figure 4. The illumination beam was generated by a single color LED located at the focal point of the first spherical mirror. The light from the LED is focused through an adjustable iris before it is reflected into the test section as a column of light. The analyzer beam is directed into a Photron SA-Z high speed camera. The camera was configured to record at 5 kHz as this was the highest frame rate that the camera could record at a full resolution of 1 MP while having enough memory to capture the full one second pulse. Each frame was exposed for 10 μs which is sufficiently short enough to temporally freeze the jet flow and leave a neutral background exposure around the schlieren. The knife-edge that exposes the transverse gradients of the schlieren is oriented in the horizontal direction to promote contrast in the axial density gradients of the flow.

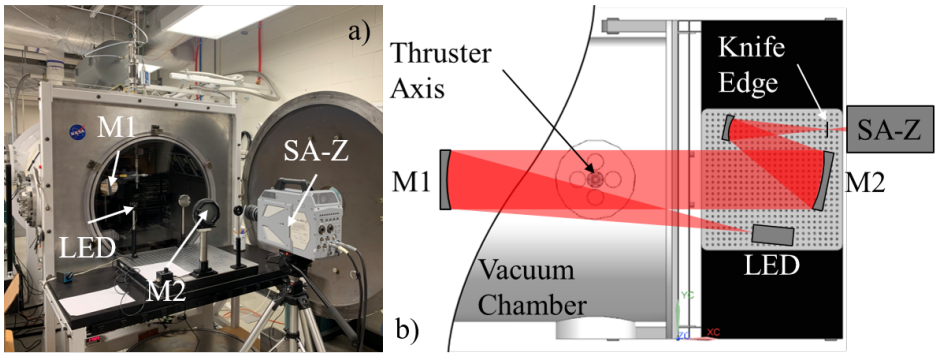

Fig. 4 a) Z-type schlieren configuration for imaging supersonic underexpanded jet impingement. b) Top-down view of optical layout of the illumination and analyzer arms of the Z-type schlieren setup.

IV. Procedure

The impingement plate is initially mounted in the vacuum chamber and the nozzle exit is zeroed on the surface of the plate. The plate is then roughly centered on the nozzle axis by carefully measuring the distance between the nozzle wall and the edge of the plate at multiple locations. This does not guarantee that centering is adequate, which is why what follows is a series of sub-atmospheric impingement tests. Any concentricity error present in the mounting location of the plate will manifest as a non-symmetric wall pressure distribution about the nozzle centerline.

Once the plate is adequately centered relative to the nozzle, the vacuum chamber is pumped down to the desired ambient pressure and the cold gas thruster is translated to the desired impingement height. While under vacuum, the schlieren setup is checked for misalignment that might have been generated during pumping and corrected. Background and flatfield images of the test region are taken for later schlieren post-processing and image cleaning. At this point the cold gas thruster is pulsed for one second. Simultaneously, the stagnation pressure P_0 and the vacuum ambient pressure P_{amb} are recorded in order to compute the theoretical jet pressure ratio as a function of time.

Synchronization among the solenoid control system, the impingement plate pressure transducer data acquisition, and the high speed schlieren acquisition is managed by a pseudo-real-time program running on a National Instruments PXI chassis. This program initiates an electronic signal that triggers the solenoid valve to open and simultaneously triggers the high speed camera to begin recording. The internal clock of the Photron SA-Z camera that governs the global shutter is routed to the data acquisition chassis so that each cycle of the clock starts the exposure of a frame and samples all five pressure sensors simultaneously.

V. Results and Discussion

Results gathered from impingement tests at 15 nondimensional heights and two jet pressure ratios are presented in this section and serve to highlight the surface dynamics that occur in plume-surface impingement interactions. These results are formatted to juxtapose Martian and Lunar terminal descent, two planetary bodies that are of interest to plume surface interaction community, as well as to characterize changes to the wall pressure distribution along a cross section of the terminal descent profile.

A. Flow Unsteadiness and Transients

A quasi-steady state flow instability was measured to be occurring at the centerline of the impingement surface, directly beneath the plate shock. This phenomena was detected at an impingement height of $h/D_e = 2$, for both the Lunar and Martian atmospheric cases with similar behaviors. As shown in Figure 5, the flow transient was measured to have a peak-to-peak pressure difference of 5.3 kPa and a constant frequency of 5.5 Hz for both jet pressure ratios tested. This low frequency fluctuation has been observed in similar supersonic jet impingement studies [7] and is attributed to the high pressure, turbulent environment in the stagnation bubble located beneath the plate shock wave. The periodic formation and dispersion of the stagnation bubble has been previously measured at between 1-10 Hz [8] which matches the fluctuations measured in this study. This transient could not be visually resolved in the schlieren photography, most likely due to the small density gradients in the stagnation bubble.

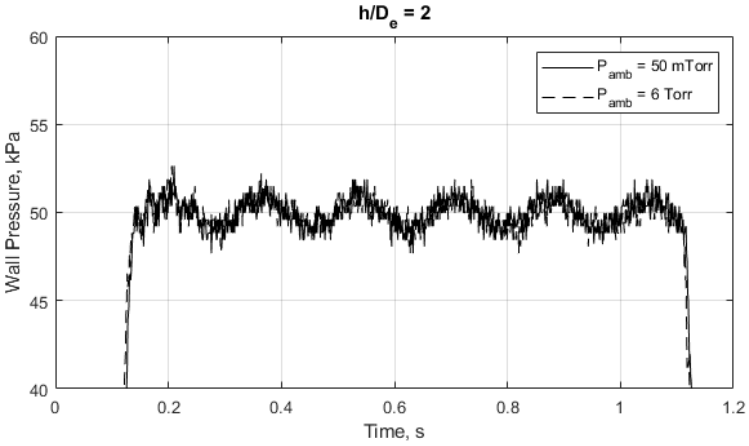

Fig. 5 Low frequency flow transient behavior encountered at h = $2D_e$ at the centerline pressure sensor.

Static wall pressure traces revealed three distinct features or regions in the behavior of the impingement pressure. The first is a startup transient peak, a short period of high impingement pressure, associated with the opening of the thruster but before the flow reaches steady state. The second feature is a long period of steady state wall pressure and is associated with the impingement flow reaching an equilibrium state. The last feature is a final transient pressure peak, located at the trailing edge of the one-second jet pulse, and is associated with the closing of the thruster and the collapsing jet structure. This is shown in Figure 6, a representative wall pressure trace of the centerline pressure sensor. The centerline wall pressure is plotted in time alongside the stagnation pressure in the nozzle plenum, which serves to demonstrate that the transient peaks are coincident with the opening and closing of the thruster's solenoid valve.

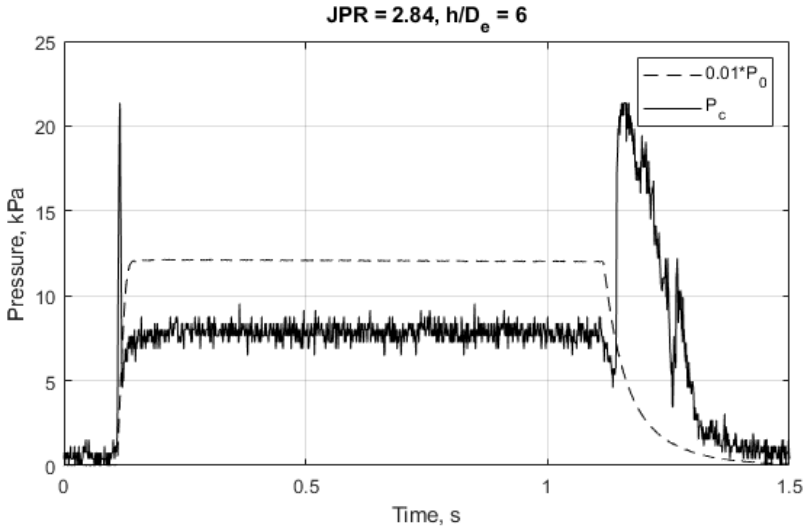

Fig. 6 Start up and shut down transient wall pressure measurements at the nozzle centerline with h = 6D_e and JPR = 2.84. The plenum stagnation pressure (P_0) is superimposed onto the plot over the wall pressure measurement (P_c)

For tests performed under Lunar atmospheric conditions, only one centerline pressure spike was measured at the trailing edge of the thruster pulse for h/D_e of between 6 and 15. Pressure peaks were measured to have an average amplitude of between 6.1 and 8.8 kPa or <1% of the thruster stagnation pressure and average durations of between 28 and 172 ms. However; for our Martian impingement application, two centerline pressure spikes were measured at the leading and trailing edge of the pulse for h/D_e of 6-9 and 13-15. Maximum ground pressure peaks for Martian impingement were in the range between 17.2 and 39.7 kPa, $\approx$ 2.5% of P_0, and durations between 7 and 19 ms at startup and 38 and 134 ms at shutdown. The asymmetric peak duration times for the Martian experiments is attributed to the asymmetric rise/fall rate of the nozzle stagnation pressure as shown in Figure 6. Wall pressure peaks at h/D_e of between 10-12 were not observed in the Martian atmosphere due to the high quasi-steady state wall pressure loading on the centerline as will be discussed in Section B. Martian impingement transients have been measured to be more sensitive to changes in the impingement height than Lunar transients, as shown in Figure 7.

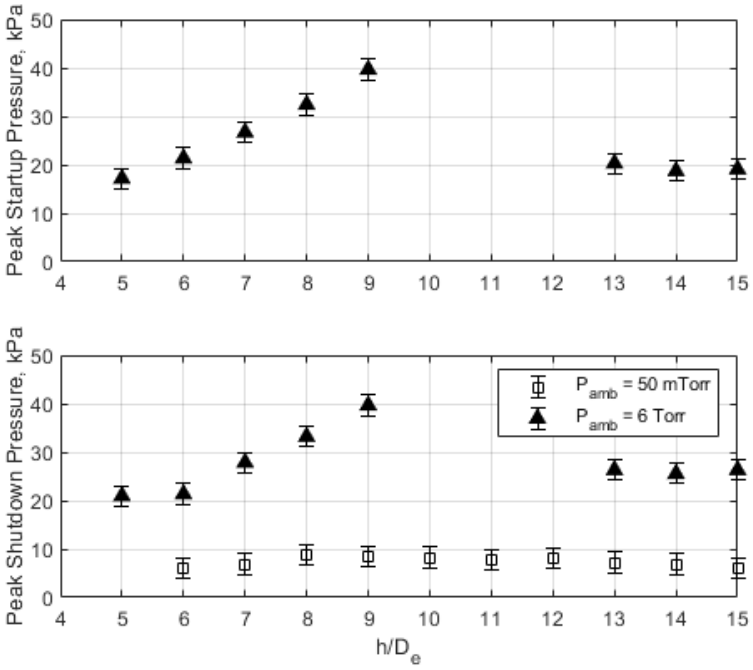

Fig. 7 Peak unsteady transients for Lunar and Martian applications along 15 increments of the non-dimensional altitude h/D_e

B. Quasi-Steady Flow Structure

Wall pressure data from the quasi-steady state region of the pulse show the average dynamic flow behavior of both Lunar and Martian jets as they descend upon to their respective landing surfaces. At Lunar conditions, steady state wall pressure increases monotonically from 482 Pa to 74.01 kPa as the nozzle exit approaches the ground target. Martian impingement test results shows two peaks in the steady state wall pressure, as seen in Figure 8, which are located at h/D_e = 1 and 10 with amplitudes of 75.91 and 45.32 kPa, respectively.

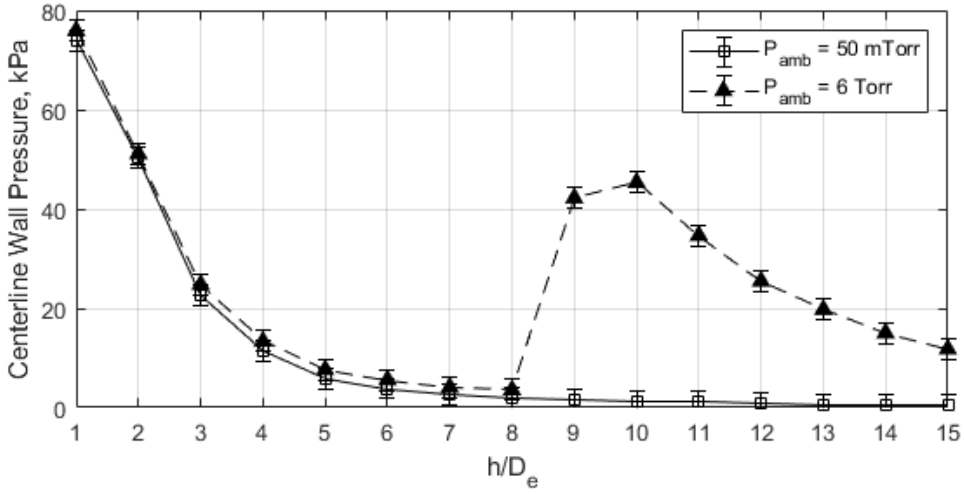

Fig. 8 Steady-state centerline wall pressure vs. impingement height at Lunar and Martian atmospheric conditions

A brief review of impingement flow dynamics is presented to differentiate the Lunar from the Martian plume structures. At startup, highly underexpanded Lunar flow with JPR $\gg 1$ is heavily processed at the exit of the nozzle through strong expansion fans that generate a large radial velocity component in the flow out towards the free pressure boundary. This jet boundary is spatially larger than that of a Martian underexpanded flow and is due to the Lunar plume requiring more expansion in order to reach a pressure equilibrium with the lower ambient atmospheric condition on the Moon at the boundary slip line. Expansion fan reflections off the pressure boundary coalesce into a Mach disk far downstream of the nozzle exit. Flow visualization studies by Wilkes [9] have shown that free flow expansion of our Mach 5 nozzle in the Lunar atmosphere would place the Mach disk significantly outside of the range of the impingement height test envelope. As a result, for h/D_e = 1-15, gas exiting the nozzle is expanded and directly impinges upon the plate, forming a stable surface shock. The large radial velocity component of the flow reduces the gas momentum flux along the nozzle axis direction and results in curved surface shocks, absent of startup transient spikes, that both decelerate the axial flow component and dissipate the impinging flow into the surrounding wall jet. At shutdown, the reflected compression waves that form the surface shock on the plate are weakened and collapse, exposing the ground to direct gas impingement and increasing the centerline gas pressure. Images of the startup and shutdown of the jet in Lunar atmospheric conditions is shown in Figure 9. The slow development of the curved surface shock agrees with the lack of a startup transient peak detected in the Lunar test cases.

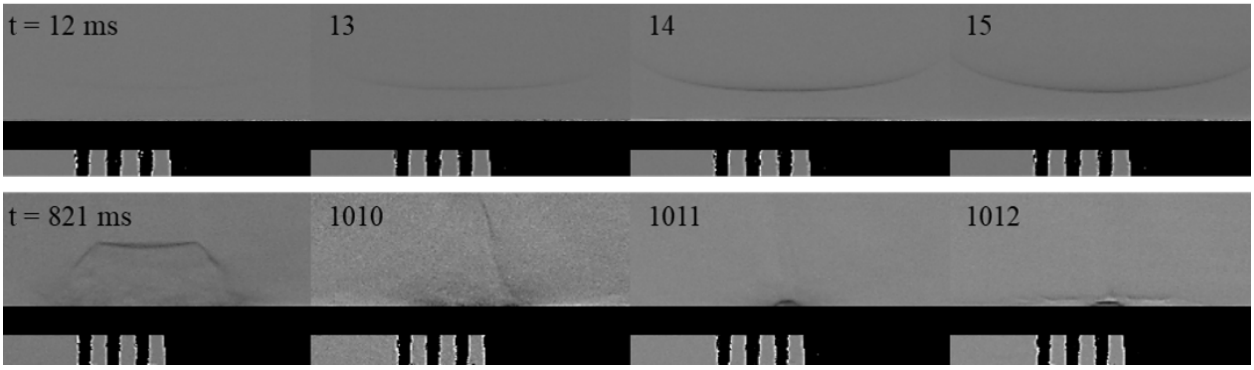

Fig. 9 Schlieren images of a Lunar impingement at h/D_e = 10. The top image sequence occurs at jet start up while the bottom sequence occurs at jet shutdown.

Similarly, moderately underexpanded flow with JPR = 2.84, such as our Martian atmosphere test condition, is expanded outward in the radial direction at the nozzle exit by an expansion fan. As stated previously, the jet boundary in this case is comparatively smaller than the Lunar case. This allows expansion waves to reflect from the pressure boundary and coalesce as oblique shock waves, located within the impingement altitude envelope of h/D_e = 1-15. The location of impingement surface within this shock cell, and by extension the nozzle exit, results in three forms of steady-state plate-shock impingement dynamics. These types are highlighted in Figure 10. The first form exhibits a surface shock above the plate. At h/D_e = 3, the flow expands into the impingement plate without the presence of a Mach disk, being processed by a surface shock wave and dissipated through the wall jet. The second form exhibits a Mach disk upstream of the ground. Increasing the impingement height to h/D_e = 7 results in a decrease in centerline wall pressure. The maximum wall pressure is located at the triple shock point formed at the intersection of the outer shear layer and the plate shock. In this type of impingement, the high speed flow in the shear layer has greater momentum than the core of the flow which is decelerated by the Mach disk. The third form of the Martian impingement dynamics exhibits crossing oblique shocks wherein the flow is parallelized prior to ground impingement. The central axis streamline undergoes significant pressure recovery, resulting in a larger maximum steady state wall pressure than at h/D_e = 3 and h/D_e = 7 as shown quantitively in Figure 8. The wall pressure and flow structure exhibit a nonlinear response to the increasing height of the nozzle, leaving significant implications for the plume surface interaction field. It is likely for these moderately underexpanded jets that as the spacecraft descends upon a dusty surface, the regolith topsoil can experience multiple peaks in the pressure loading. This can lead to multiple instances of the soil bearing capacity being exceeded and the particles being lifted into the flow of the jet.

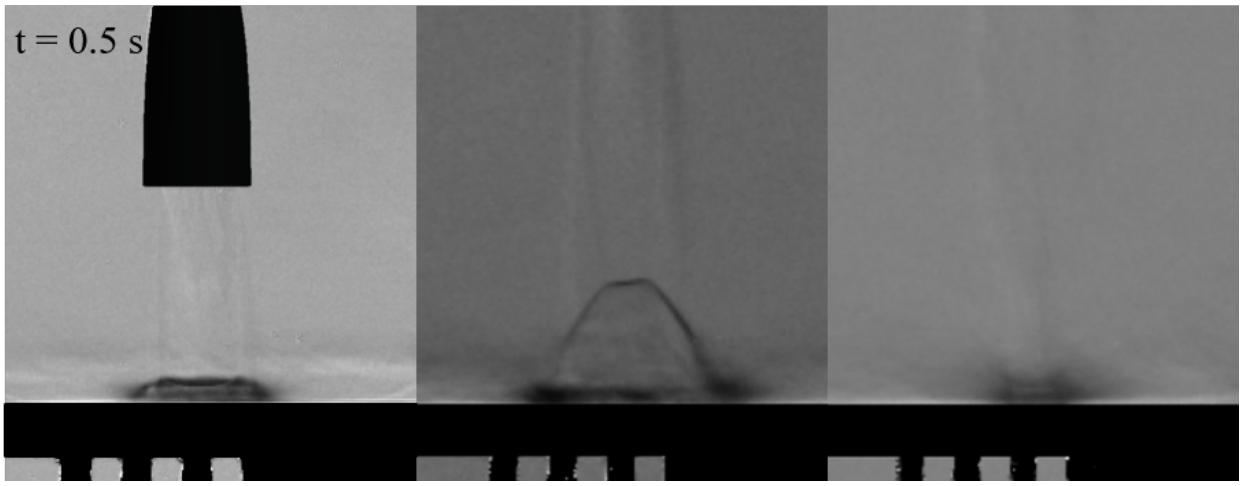

Fig. 10 Schlieren images at three impingement heights in Martian ambient conditions, (from left to right, h = $3D_e$, $7D_e$, and $10D_e$)

VI. Conclusion and Further Work

The ground pressure sensor testbed and schlieren imaging setup have shown good agreement with one another. Startup and shutdown pressure amplitudes can be strongly correlated to the formation and collapse of the surface normal plate shock. These transient responses to an underexpanded jet impinging on a solid flat surface have been measured at impingement heights ranging from one to fifteen nozzle exit diameters. Quasi-steady state ground pressure measurements demonstrate that at moderate jet pressure ratios, the terminal descent of a lander can impart a surface pressure loading that has multiple maxima and is sensitive to the impingement height and corresponding shock structure interactions with the ground.

This study will expand by upgrading the impingement pressure instrumentation in order to improve the spatial resolution of the wall pressure distribution. A higher spatial density of ground pressure sensors will help us to better resolve the dynamics of the stagnation bubble, and dynamics beyond the region below the plate shock. Additionally, to reduce uncertainty in the boundary conditions at the nozzle, a molecular tagging velocimetry experiment will be used to accurately measure the true gas velocity at the exit of the nozzle.

Acknowledgments

This material is based upon work supported by NASA under grant No. 80NSSC20K0304 issued through the Early Stage Innovation Program. We would like to acknowledge the support of our research collaborators from Langley Research Center Dr. Paul Danehy and Dr. Neil Rodrigues. Any opinions, findings, and conclusions or recommendations expressed in this material are those of the authors and do not necessarily reflect the views of the National Aeronautics and Space Administration.

References

[1] Land, N. S., and Clark, L. V., "Experimental investigation of jet impingement on surfaces of fine particles in a vacuum environment." 1965.

[2] Plemmons, D. H., "Effects of the Phoenix Lander descent thruster plume on the Martian surface," *j. Geophys. Res. E Planets*, 2009, p. 114.

[3] Rao, G. V. R., "Exhaust Nozzle Contour for Optimum Thrust," *Journal of Jet Propulsion*, Vol. 28, No. 6, 1958, pp. 377–382.

[4] Mehta, M., Renno, N., and Cotel, A., "Characterization of the Impingement Dynamics of Pulsed Rocket Plumes with the Ground at Low Ambient Pressure," *AIAA Joint Propulsion Conference Exhibit*, 2007.

[5] Anderson, J. D., *Modern Compressible Flow: With Historical Perspective*, 3rd ed., McGraw-Hill, Boston, 2003.

[6] Settles, G. S., *Schlieren and shadowgraph techniques: Visualizing phenomena in transparent media*, Springer, University Park, PA, 2013.

[7] Gubanova, O. I., Lunev, V. V., and Plastinina, L. I., *Fluid Dyn.*, Vol. 6, 1974, p. 135.

[8] Kalghatgi, G. T., and Hunt, B. L., *Aero. Quart.*, Vol. 27, 1976, p. 169.

[9] Inman, J. A., Danehy, P. M., Nowak, R. J., and Alderfer, D. W., "Fluorescence Imaging Study of Impinging Underexpanded Jets," *AIAA Aerospace Sciences Meeting and Exhibit*, 2008.